AERO 405: Team SIMPly Hartl
Final Report

Hunter Ducharme, Stephanie Estrada, Dominic Lira, Carter Long

Abstract

Supersonic transports (SST) are aircraft capable of transporting civilians at speeds exceeding Mach 1, or faster than the speed of sound. In the past, supersonic aircraft, such as the Concorde and the Tupolev Tu-144, were too expensive to keep operational. Production costs were high, which in turn caused the price of tickets to rise. This project addresses this problem by designing and optimizing a variable-swept wing for a supersonic jet transport. The wing was optimized by minimizing its mass and constraining the magnitude of deflection at the wingtips. Five different design variables were chosen as opportunities to optimize: number of ribs, thickness of ribs, radii of circles, thickness of spars, and skin thickness. These variables were varied to find the best design possible for a supersonic transport. The design space for each variable was limited using a Taguchi design of experiments (DoE) and interpreted to determine the relationships between variables. The design was then optimized using a genetic algorithm to minimize the mass and deflection of the proposed wing. To simulate the loads experienced by the wings during supersonic flight, a spanwise and chordwise elliptical load distribution was applied to the model. For the purposes of this report, the main difference between subsonic/supersonic wing loading is the respective magnitude of the load for each case. ABAQUS was employed to analyze the structural strength of the wing required to be successful in withstanding the imposed loads: a takeoff loading case and a supersonic cruise loading case. It was found that the wing, even with reduced bounds, is still strongly overengineered (an unintended consequence from the wing being composed of merged parts, as opposed to tied).

Design Problem

The wing is comprised of four main components:ribs,stringers,skin,and spars.

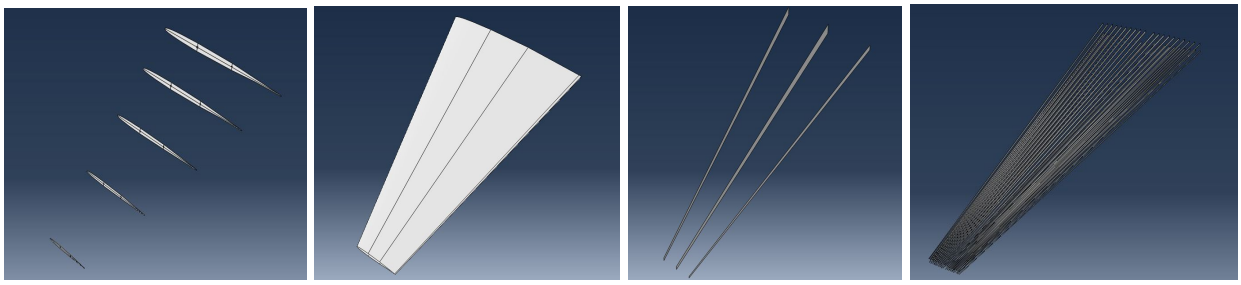

Figure 1: (From left to right)-Ribs, Skin, Spars, and Stringers

The main reason why the spars/stringers are limited to the "middle" section of the wing (**Figure 3**) is because the front portion is dedicated to leading edge slats, while the portion near the trailing edge is dedicated to flaps and ailerons (all of which were not modeled, as they are not load bearing components). This limits stringer/spar location to between 0.15c-0.75c.

The materials that make up the structure are Aluminum 7075 and a composite layup that emulate an 8-ply (at the respective orientation angles per layer: 0°, 90°, 45°, -45°, -45°, 45°, 90°, 0°) carbon fiber/epoxy layup. The ribs, stringers, and spars are Aluminum 7075. The skin is made of the composite layup. The table below details the material properties.

Aluminum 7075			Composite Layup (Carbon/Epoxy AS4/3501)				
Density ($\frac{lb}{in^3}$)	Young's Modulus (psi)	Poisson's Ratio	Density ($\frac{lb}{in^3}$)	E1 (psi)	E2 (psi)	v12	G12 (psi)
0.102	1.04e7	0.33	0.057	2.06e7	1.49e6	0.27	1.04e6

Figure 2: Material Data

Our wing anticipates relatively high loading (0.3-0.375 psi wing loading), so choosing a material with high strength (and a good strength-to-weight ratio) was critical, leading us to choose to make the spars,stringers, and even ribs out of Aluminum 7075. Arguably, ribs and stringers didn't need to be made of Al 7075, but we kept it that way to ensure material uniformity and allow for a stiff wing (under the effect of torsional/bending loads).

Initially, Aluminum 2024 was selected to be the material of the skin, due to its strength across a wide range of temperatures (including high temperatures, which the wing would presumably encounter at supersonic speeds). However, our early models showed that our skin would have to be ~0.4-0.5 inches thick in order to not encounter an immense amount of deflection. Thus, the composite layup was used, as it can sustain its layup at high temperatures as well, while maintaining desirable strength/weight properties.

After the parts were defined, they were merged together to give the wing as shown below.

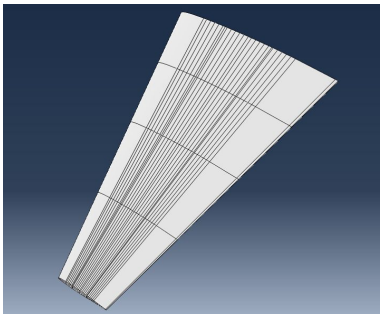

Figure 3: Merged Wing

The wing had an elliptical pressure load across the wingspan (**Figure 4**), which followed the equation $L = Lo\sqrt{1-(\frac{z}{b/2})^2}$ (where Lo is the lift at the root, z is in the direction of the wingspan, and b is whole wingspan). The magnitude of the pressure loading for the subsonic case and the supersonic case were 0.306 psi and 0.375 psi, respectively. Due to a geometry error near the wingtip, the elliptical load was applied across a majority of the wingspan (a function of the number of ribs). The area near the wingtip was applied a pressure load that was evaluated as 5% of the maximum wing loading. In real life, the wing experiences a majority of the loading at the aerodynamic center (assumed to be c/4 in our case). To emulate the drop in pressure near the trailing chord, the elliptical loading was decreased to 10% of its magnitude (**Figure 5**).

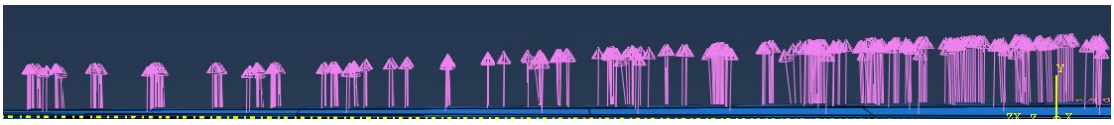

Figure 4: Wing Loading Across the Wingspan (Loading Not to Scale)

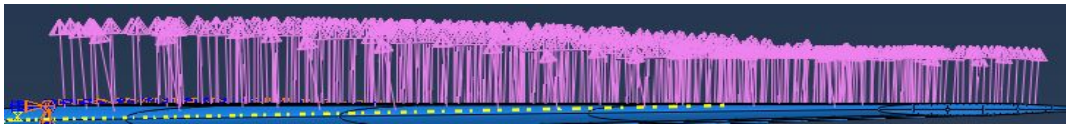

Figure 5: Wing Loading Across the Chord (Loading Not to Scale)

Since we're primarily interested in general stress contours (no emphasis on localized stress) and deflection, the mesh is comprised of structured S4R and S3 elements, with a global seed size of 3 (**Figure 6, left**). Initially a larger seed was used but a seed size of 3 was chosen to prevent any aborted jobs as the DOE/optimization scripts ran. The ribs were partitioned vertically/horizontally across their respective holes to help with mesh quality (**Figure 6,right**).

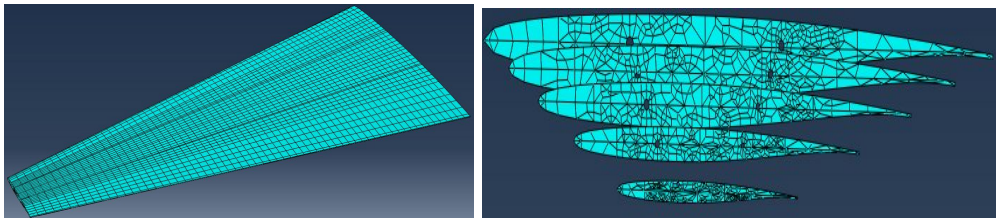

Figure 6: (Left):Meshed wing skin; (Right): Meshed Ribs

The root chord was encastred at the root chord (**Figure 7**). Symmetry conditions allowed for only half of the total wing to be modeled, with the assumption the encastred region is infinitely strong and that both wing halves behave the same.

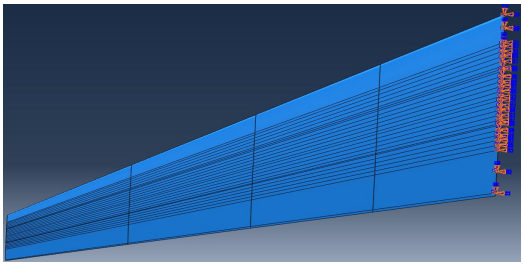

Figure 7: Encastered boundary condition

The selected design variables are chosen from the components of the structure itself, listed below with respective bounds (**Figure 8**). The output variables are total mass (lbs), wingtip deflection (in), max stress (psi), and total rib mass (lbs). The constraints are a yield stress of 73,000 psi, a deflection of 8 inches (subsonic case), and a deflection of 10 inches (supersonic case).

Design Variables					
	Number of Ribs	Rib thickness (in.)	Hole diameter (% of local rib chord)	Spar Thickness (in.)	Skin Thickness (in.)
Minimum Value	5	0.03	0.25	0.5	0.05
Maximum Value	30	0.2	0.5	2.0	0.5

Figure 8: Design Variables

Analytical Model

Description

An analytical model for our wing is very difficult to extract due to the large number of different parts and design variables. In order to survey the effects of changing design variables, before we actually had our Abaqus model running, an analytical taguchi was performed to see factor effects on weight, stress, and deflection. In order to approximate the weight, rough estimates of each component were necessary. Rib weight was approximated as:

$$w_{ribs} = \rho_{Al-7075} * n_{ribs} * t_{ribs} * (mean\ chord\ length * mean\ chord\ height - 3 * \pi * r_{cutout}^{2})$$

Where mean chord length is the length of the mean chord, and mean chord height is the height of the mean chord. This overapproximates the rib mass because the ribs are modeled to be rectangular. Spar weight was approximated as:

$$w_{spars} = 3 * \rho_{Al-7075} * t_{spars} * mean\ chord\ height * wingspan/2$$

This approximates the spars as equal length and height which is not true in the real model, giving an overestimate of spar weight. Finally, skin weight was taken to be:

$$w_{skin} = \rho_{AS4/3501} * A_{wing} * t_{skin}$$

Due to the fact that the skin thickness is so small, wing area was approximated as constant throughout the thickness, when in fact it is smaller on the inside of the skin than the outside giving a slight overestimate on weight.

In order to capture the effects on the tip deflection, a simple Euler-Bernoulli approximation was made on the three spars with their dimensions assumed the same as in the calculation of weight. The loading on the spars was modeled as equally distributed along the three and along the length of the spars. The total loading was taken to be equal to half the aircraft weight as is roughly the case in steady, level flight (for one wing).

While this model is very low fidelity, it provides limits on our performance metrics that are considered acceptable. If we took the analytical model more seriously, we might have actually caught on that it was over-engineered earlier due to the high weights and low deflections that we got from it.

Results

n_ribs	t_ribs	r_cuts	t_spars		t_skin	weight	deflection	stress
15.00	0.03	0.25	1.50	0.15	38076.37		0.65	1238461.65

Figure 9: Sample case from Analytical Approximations

Design of Experiments

Description

Before we begin the optimization of our wing, we have to determine the effects of our design variables on our outputs. To limit our design space for our project, we chose to use a Taguchi L16 array. This is due to the large number of design variables we are considering, and because Taguchi is a balanced 4-level DoE approach. Factorials work by considering all combinations of design variables at all levels. Taguchi design experiments rely on the smallest fractional factorial possible that still produces results that are statistically significant. We believed that using a Full Factorial would be too expensive to run for our project, so we instead chose Taguchi for its ability to reduce computational time. Using the data acquired from our Taguchi array we created factor effects plots. Factor effects plots show the relationships between output variables and design variables. Based off of how the trends behaved on these factor effects plots and what relationships were shown we were able to determine if we needed to eliminate or alter any of our variables used throughout this project.

Results

Below are the Taguchi tables and Pareto Frontiers for respective subsonic and supersonic cases, as well as examples of "good" (highlighted in yellow) cases and "bad" cases (highlighted in red). **Figure 15 (**and **Figure 22)** is an example of "bad" cases, since there's significant stress and deformation near the wing's root (both undesirable characteristics). **Figure 16** (and **Figure**

23) show “good” cases, because it has a more realistic stress distribution and has favorable deformation performance (more on this in the conclusion).

Runs	n_ribs	t_ribs	r_cuts	t_spars	t_skin	Mass Total (lbs)	Deflection (in)	Stress (psi)
1	5	0.030	0.250	0.500	0.050	1762	17.97	49615.15
2	5	0.0870	0.333	1.000	0.200	4665	5.62	13276.59
3	5	0.143	0.417	1.500	0.350	7568	3.33	5984.92
4	5	0.200	0.500	2.000	0.500	10469	2.36	3353.81
5	13	0.030	0.333	1.500	0.500	9462	3.15	5298.63
6	13	0.087	0.250	2.000	0.350	8534	4.10	3609.45
7	13	0.143	0.500	0.500	0.200	4013	7.72	6577.61
8	13	0.200	0.417	1.000	0.050	3085	18.70	14199.85
9	22	0.030	0.417	2.000	0.200	6493	6.38	5135.41
10	22	0.087	0.500	1.500	0.050	3854	15.88	20408.00
11	22	0.143	0.250	1.000	0.500	9053	3.26	2265.68
12	22	0.200	0.333	0.500	0.350	6416	4.71	3500.37
13	30	0.030	0.500	1.000	0.350	6696	4.55	4411.89
14	30	0.087	0.417	0.500	0.500	8052	3.40	2604.45
15	30	0.143	0.333	2.000	0.050	5173	13.82	17318.98
16	30	0.200	0.250	1.500	0.200	6536	6.78	4647.99

Figure 10: Taguchi L16 - Subsonic Case

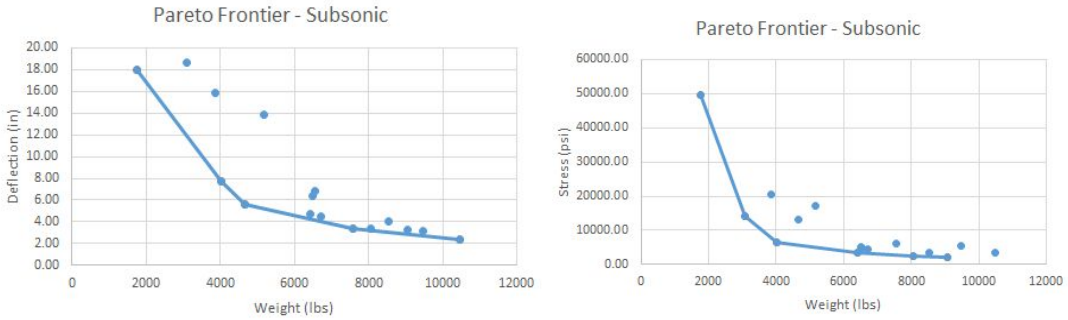

Figure 11: (Left) Deflection vs Weight; (Right) Stress vs Weight

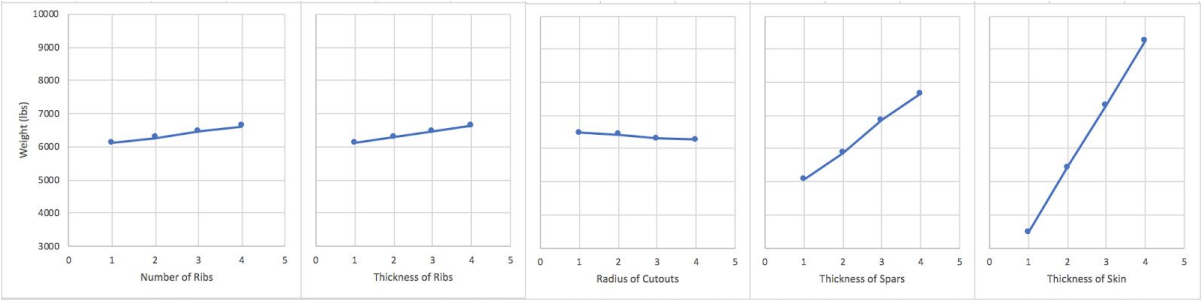

Figure 12: Factor Effects - Weight

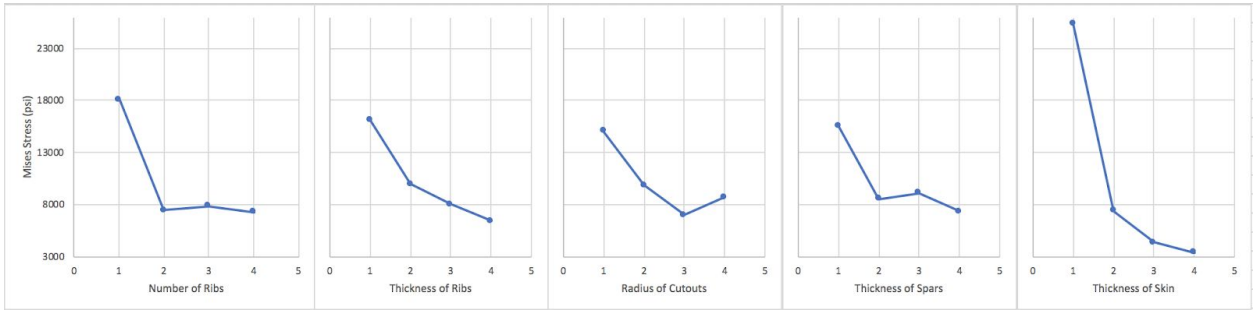

Figure 13: Factor Effects - Mises Stress

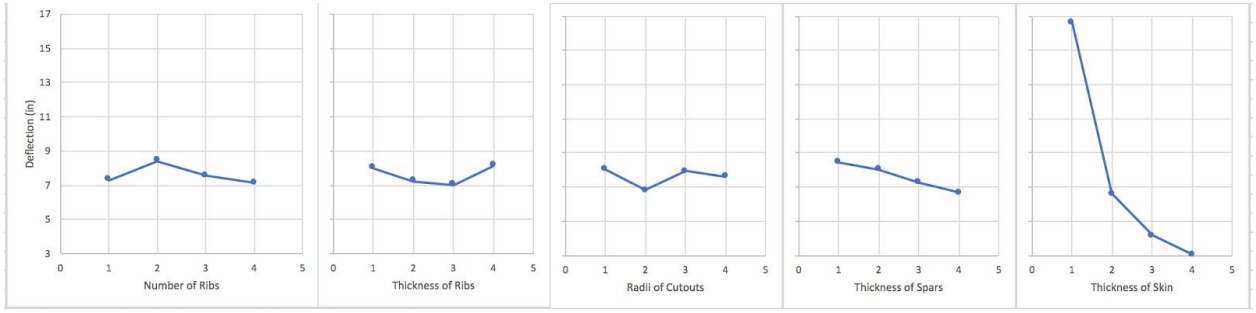

Figure 14: Factor Effects - Deflection

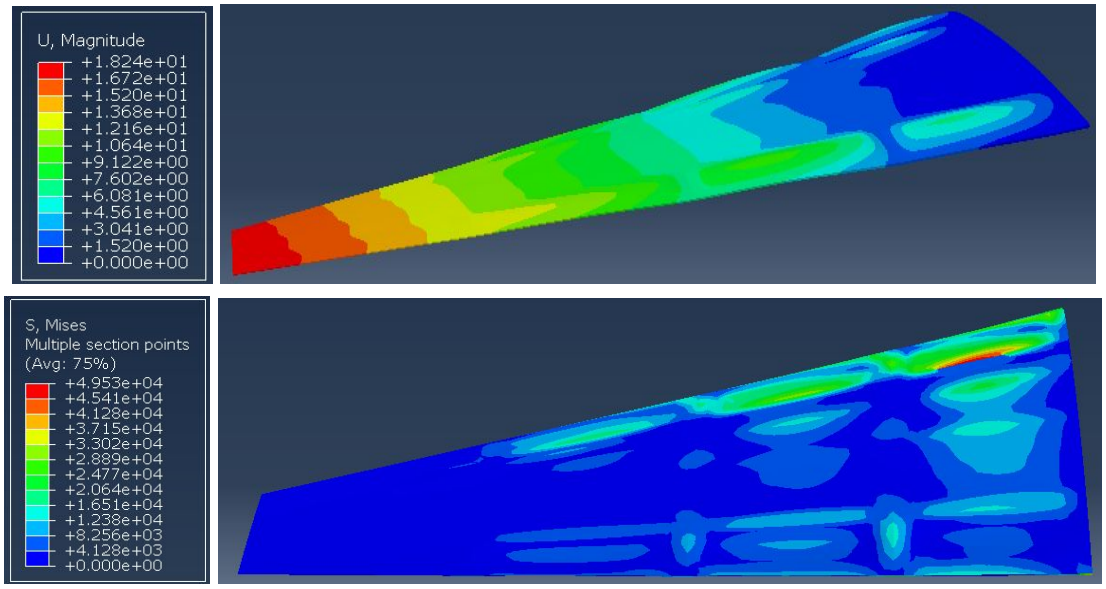

Figure 15: A "Bad" Case for Subsonic; (Top)-Deflection;(Bottom)-Stress

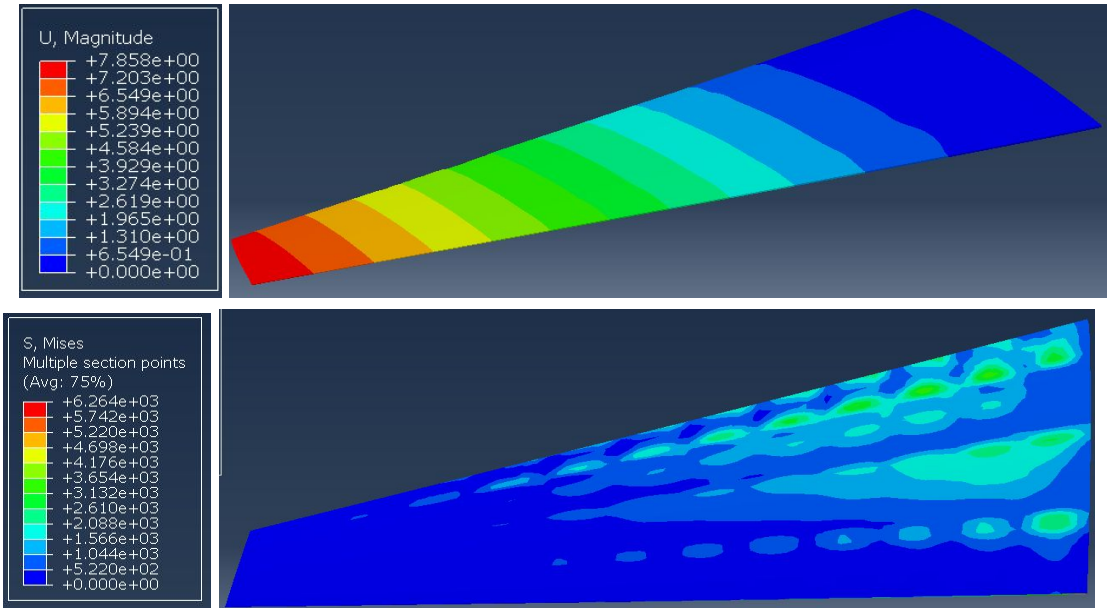

Figure 16: A "Good" case for Subsonic ; (Top)-Deflection;(Bottom)-Stress

Runs	n_ribs	t_ribs	r_cuts	t_spars	t_skin	Total Mass (lbs)	Deflection (in)	Stress (psi)
1	5	0.030	0.250	0.500	0.05	1762	22.46	62018.93
2	5	0.087	0.333	1.000	0.20	4665	7.03	16595.74
3	5	0.143	0.417	1.500	0.350	7568	4.16	7481.15
4	5	0.200	0.500	2.000	0.500	10469	2.95	4192.26
5	13	0.030	0.333	1.500	0.500	9462	3.94	6623.28
6	13	0.087	0.250	2.000	0.350	8534	5.12	4511.81
7	13	0.143	0.500	0.500	0.200	4013	9.66	8222.01
8	13	0.200	0.417	1.000	0.050	3085	23.37	17749.81
9	22	0.030	0.417	2.000	0.200	6493	7.97	6419.26
10	22	0.087	0.500	1.500	0.050	3854	19.85	25509.98
11	22	0.143	0.250	1.000	0.500	9053	4.08	2832.10
12	22	0.200	0.333	0.500	0.350	6416	5.89	4375.46
13	30	0.030	0.500	1.000	0.350	6696	5.68	5514.87
14	30	0.087	0.417	0.500	0.500	8052	4.25	3255.57
15	30	0.143	0.333	2.000	0.050	5173	17.27	21648.74
16	30	0.200	0.250	1.500	0.200	6536	8.48	5809.99

Figure 17: Taguchi L16 - Supersonic Case

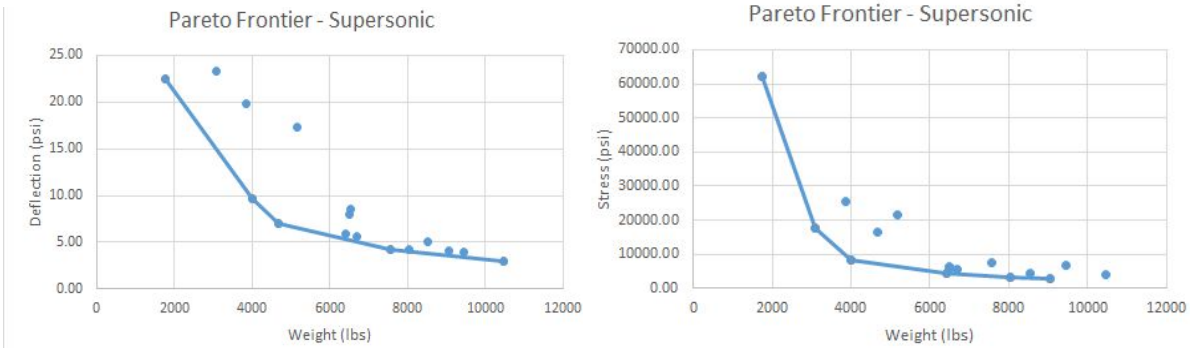

Figure 18: (Left)Deflection vs Weight; (Right) Stress vs Weight

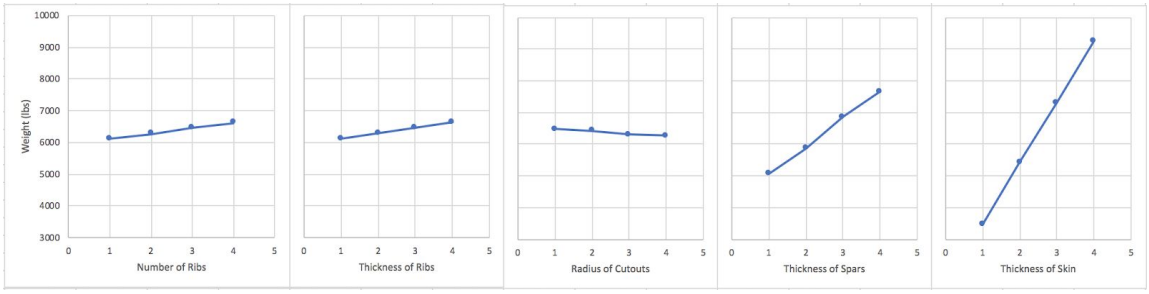

Figure 19: Factor Effects- Weight

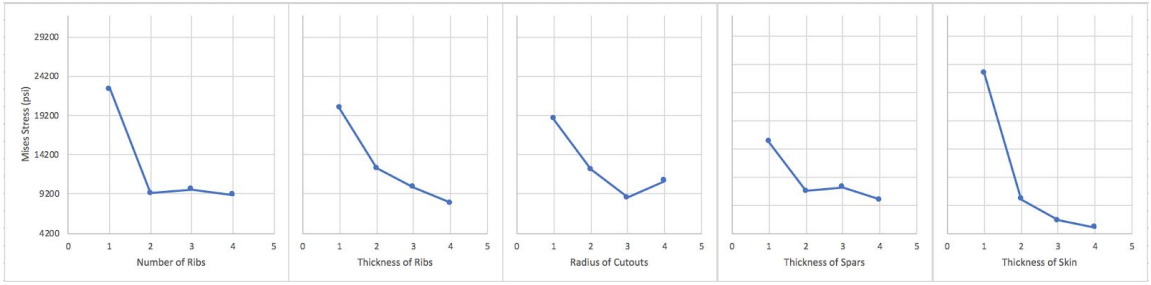

Figure 20: Factor Effects- Mises Stress

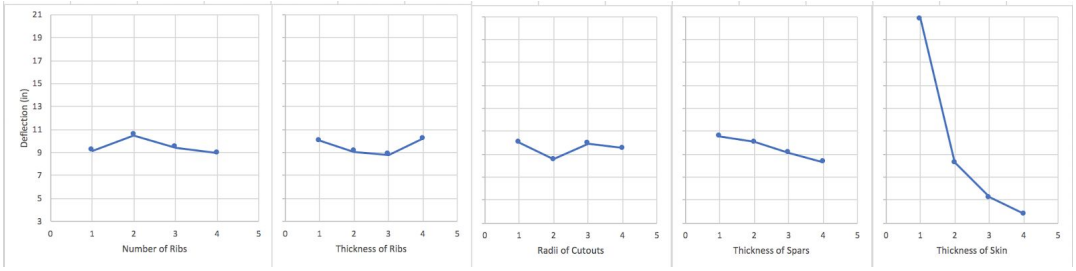

Figure 21: Factor Effects- Deflection

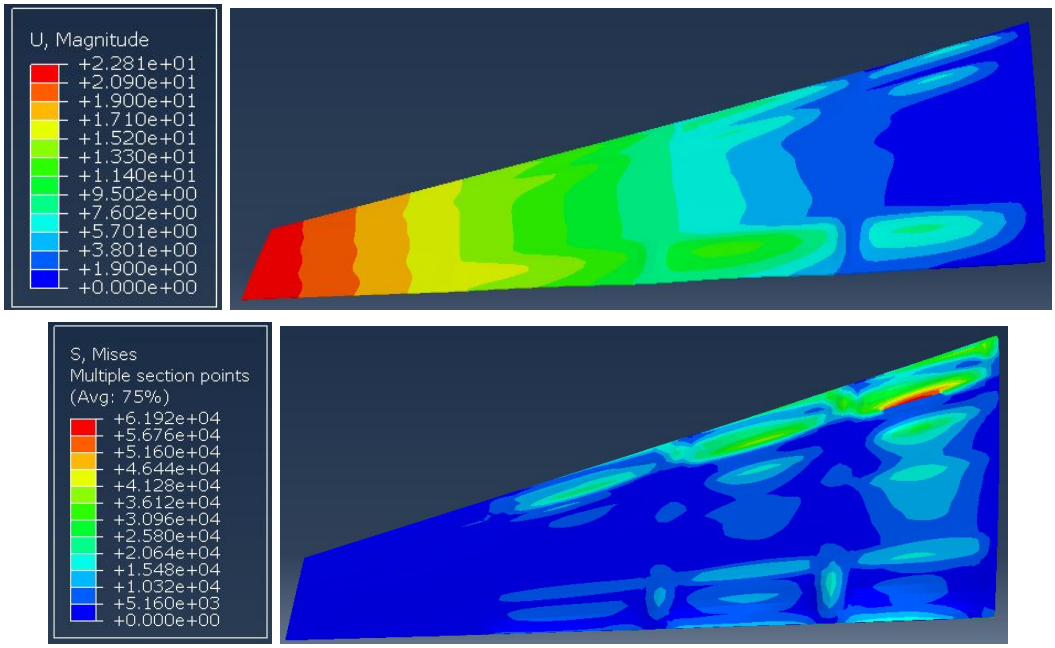

Figure 22: A "Bad" Case for Supersonic; (Top)-Deflection;(Bottom)-Stress

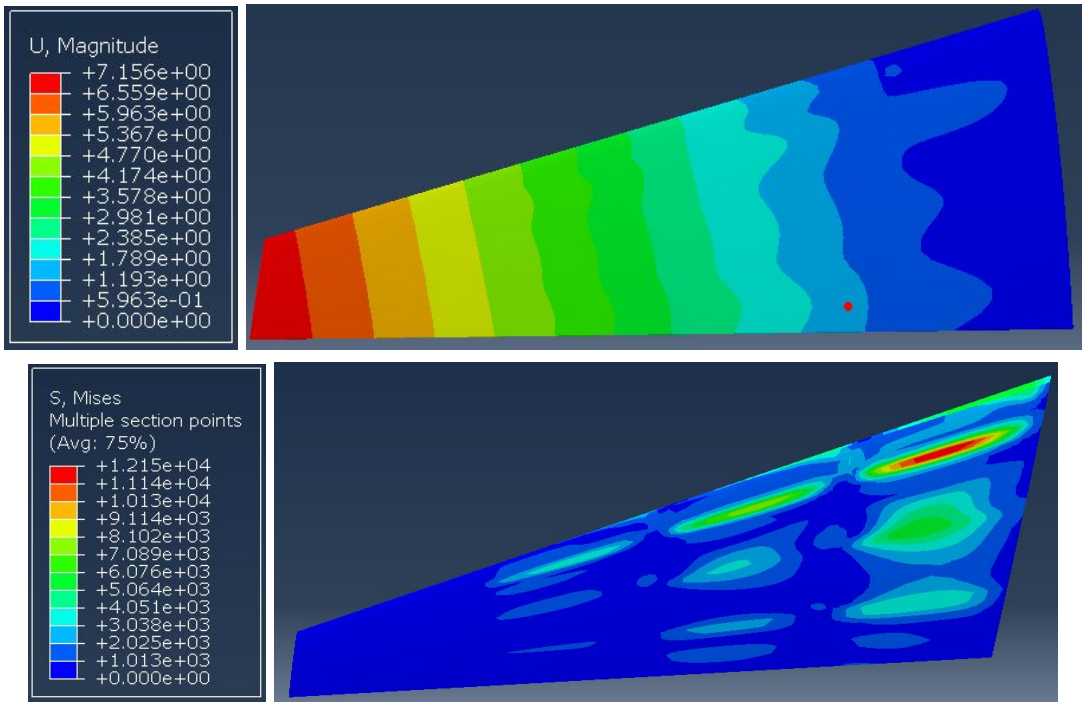

Figure 23: A "Good" Case for Supersonic; (Top)-Deflection;(Bottom)-Stress

Discussion

From these factor effects plots, you can get a good feel for how each design variable changes each of our performance metrics. While there was not much difference between the supersonic and subsonic cases, we wanted to see the effects on both just in case. The thickness of the skin appeared to be the most influential design variable in the outcome of each performance metric due to the large changes in each metric over the four different levels of skin thickness. The number of ribs decreased in importance as a DV from our previous design after we changed the bounds on our design variables to fix our over-engineered preliminary design. No design variables were eliminated as each provided sufficient change to the output variables..

Optimization

The employed genetic algorithm was benchmarked by utilizing the 2-D Rastrigin function, a non-convex function that has a large number of local minima. Below is the function:

$$Ras(x,y) = 20 + x^2 + y^2 - 10(cos2\pi x + cos2\pi x)$$

$$where\ f(x,y) = 0\ is\ the\ global\ minima$$

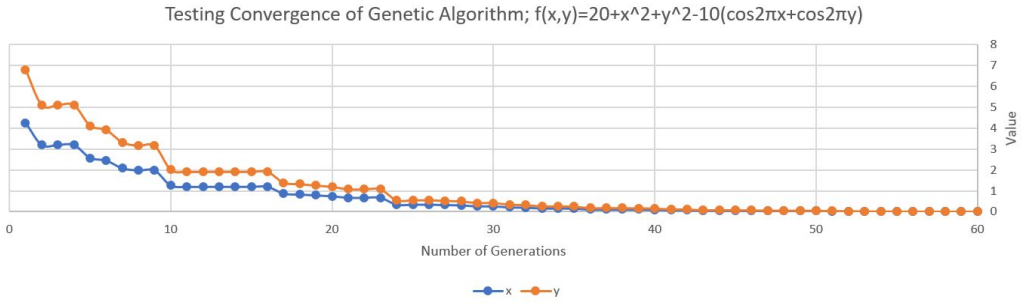

Figure 24: Convergence of Rastrigin function

After 60 generations, the initial values (x=10;y=10) converged to less than 5% of zero.This proves that our algorithm has the capability to converge with enough populations.

It should be noted that the convergence of the Rastrigin function also depends on how big the initial values of x and y are. Meaning, it converges faster the closer x and y are to zero. We emulated this idea by producing a population of 25 sets via a Latin Hyper Square. The design space was then iterated through a genetic algorithm.The constraints were to not exceed a yield stress of 73,000 psi as well having a small deflection: a maximum of an 8 inch deflection at the wingtip for the subsonic (takeoff) case and a 10 inch deflection at the wingtip for a supersonic (cruise) case. Using stress/deflection constraints, the algorithm would check to see what combinations caused the structure to fail, eliminating those cases.The remaining configurations were sorted by their best and had the 5 lightest structures retained. The design variables were then mutated by variable amounts: a 67% chance of a small mutation (5%), a 20% chance of an intermediate mutation (15%), and a 13% of a large mutation (20%). The data was then assigned a "child" parameter set and before the child was passed, the mutation was checked to see if failure had occurred. This set of mutations occurred until 25 children were generated, where then the children were sorted according to lowest mass and the top performers were retained. This whole process occurred for 20 generations. Although more generations are desirable, due to the proximity of the deadline (each generation took about 50 minutes) as well as previous failures our group had running the optimization at larger seed sizes, we believe that 20 generations is enough to provide realistic results within a relatively short amount of time.

TopOpt

As a means of further decreasing the weight of the overall structure, the ribs were chosen to be topologically optimized. The rib was modeled in ABAQUS as a shell and was meshed using shell elements. The rib was partitioned in three spots along the length of the one-foot chord to represent the locations of the three spars that it would be in contact with, and was encastered at these positions. A pressure load was defined on four different edges on the perimeter of the rib (two edges on top and bottom, "Edge 1" for the front half and "Edge 2" for the back half of the), and based on the load condition the pressure magnitudes varied. The two loading cases simulated on the rib are shown below in **Figure 25**, and a visual representation of the loads and boundary conditions are shown in **Figure 26**.

	Lower Load Case (psi)		Higher Load Case (psi)	
	Edge 1	Edge 2	Edge1	Edge 2
Top of the rib	1.0	0.5	1.8	1.0
Bottom of the rib	0.75	0.4	1.5	1.0

Figure 25: Loading Scenarios

In the early stages of the rib optimization, a simple symmetrical airfoil (not the airfoil used in the wing model) was created in ABAQUS and the TopOpt results from a constant pressure loading are shown below in **Figure 27**.

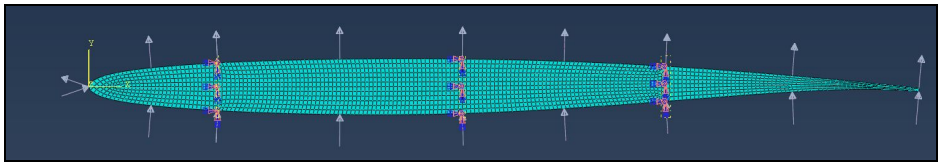

Figure 26: A NACA 0406 airfoil (encastered at three spar locations, constant loading)

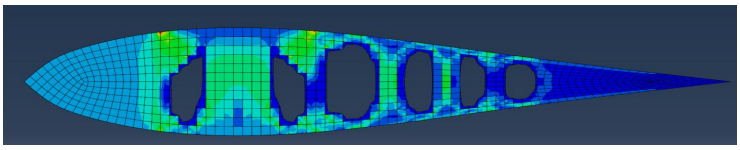

Figure 27: Optimized topology of symmetrical airfoil (constant pressure along perimeter)

This is not the airfoil used in the wing model, so more accurate FEA simulation was run on a rib from the wing model utilizing the NACA 0406 airfoil. The results are shown below in **Figures 28 and 29**.

Figure 28: The stress distributions in a NACA 0406 rib simulated for the lower loading case. (Top): Rib without TopOpt. (Bottom): Rib with TopOpt

Figure 29: The stress distributions in a NACA 0406 rib simulated for the higher loading case. (Left): Rib without TopOpt. (Right): Rib with TopOpt.

These results drove the decision to place a circle between each spar in the actual wing model, as depicted in **Figure 6 (right)**.

Results

The genetic algorithm delivered 20 generations worth of best performers, the utmost best shown in **Figure 30** and **Figure 31**. It turns out that the location of the maximum stress in the structure is at corner of the leading edge and the root chord, caused by a sharp corner in the wing. Nonetheless, the regions of practical interest lay on the topmost layer of the wing. The

areas of highest stress are near the wing's root (as anticipated), and the ideal results a typical wing deflection, albeit a small amount. However, the pareto frontiers changed unfavorably (**Figure 32. Figure 33**), with the optimization points inside of both existing frontiers.

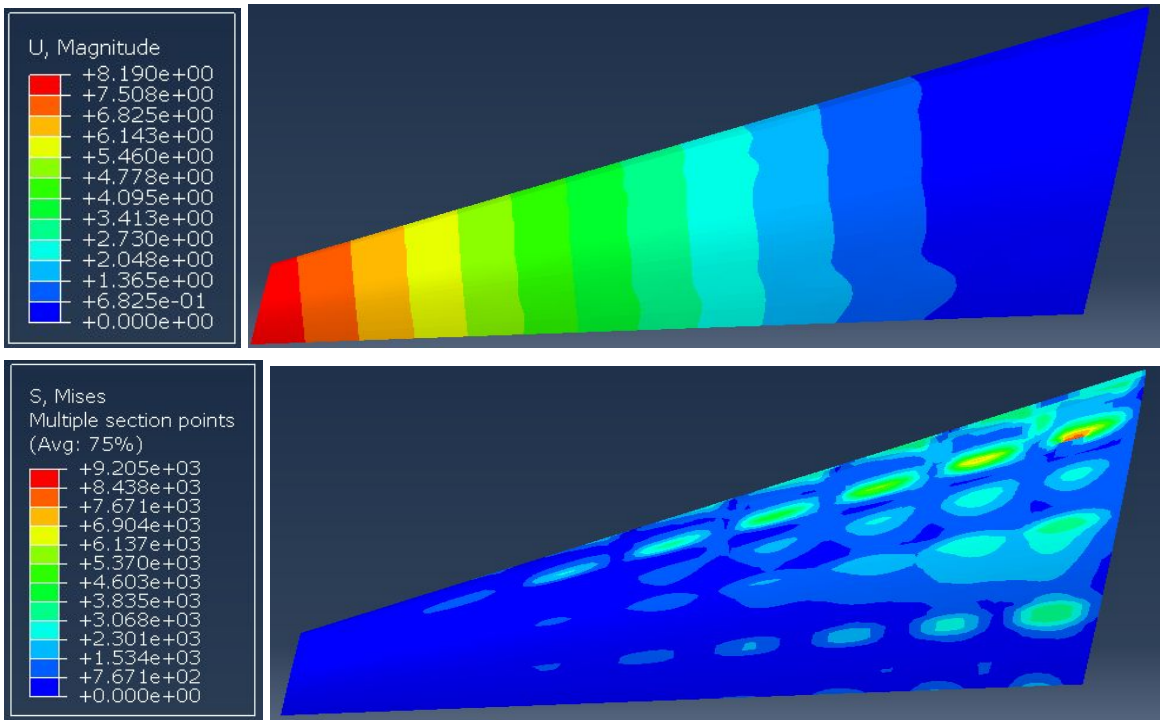

Figure 30: Optimized Model (Subsonic Case); (Top)-Deflection;(Bottom)-Stress

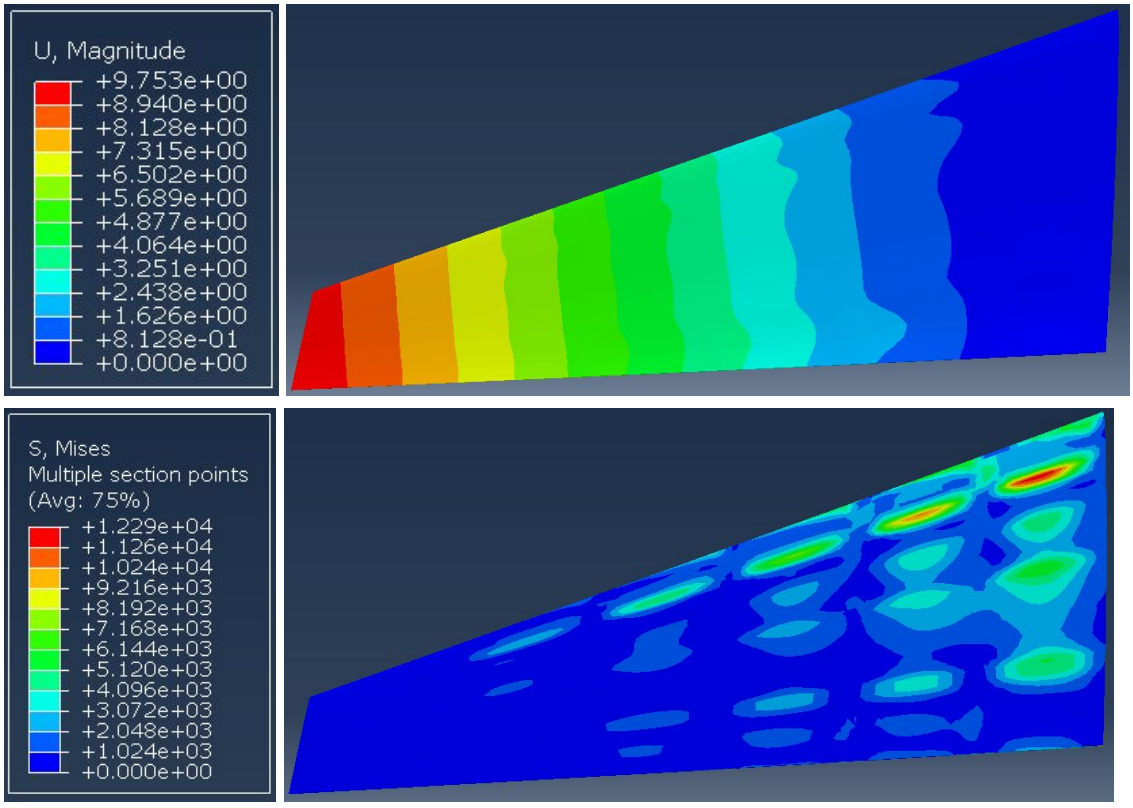

Figure 31: Optimized Model (Supersonic Case); (Top)-Deflection;(Bottom)-Stress

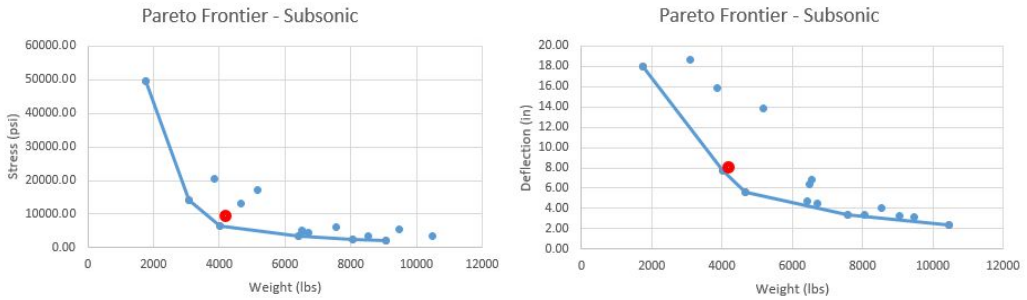

Figure 32: Updated Subsonic Pareto Frontiers (Red Dot is Optimized Design)

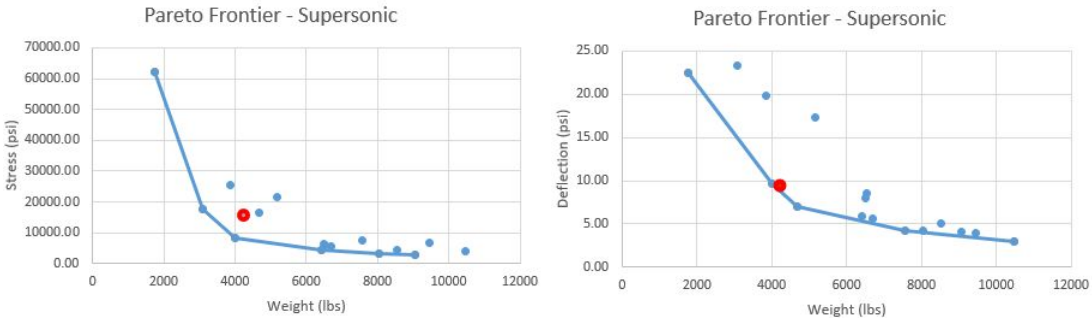

Figure 33: Updated Supersonic Pareto Frontiers (Red Dot is Optimized Design)

In order to quantify an optimized design, an objective function $\hat{f}$ was defined as a weighted function between the total mass and deflection of the system. That is, $\hat{f} = w_1(mass) + w_2(deflection)$. The optimized design is one that minimizes $\hat{f}$ more than any other design while still adhering to the constraints imposed on the model. For each generation, the mass and deflection from each child in the population were extracted and put onto a scatter plot as shown below. The deflection and mass data were normalized by the highest value in their respective data sets. The results for a 50-50 weighted function for the subsonic load case are shown in **Figure 34**, and the results for a 50-50 weighted function for the supersonic load case are shown in **Figure 35**.

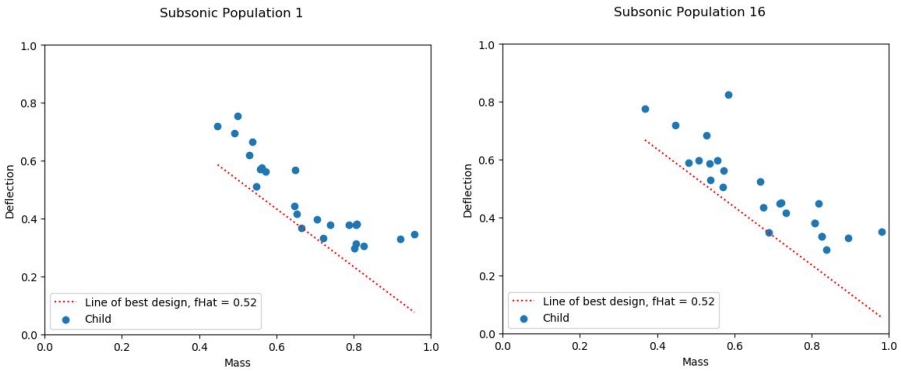

Figure 34: Subsonic data for deflection and mass with a line showing the optimized design.

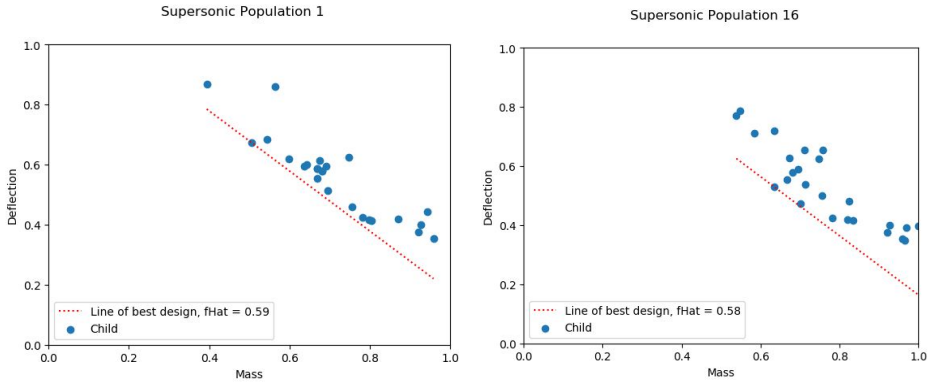

Figure 35: Supersonic data for deflection and mass with a line showing the optimized design.

From these figures it can be concluded that very little optimization is happening, if any, however, this implies the last generation is the most optimized design which is not the case due to random mutations. Generations 15 and 7 had the absolute optimal design for the subsonic and supersonic cases, respectively. As seen in the animations sent via email, the best designs tend to hover in the same region around the same $\hat{f}$ value. **Figure 36** shows the statistics of the objective function for both cases.

	Minimum Value	Maximum Value	Mode	Standard Deviation
Subsonic	0.51	0.53	0.52	8.1×10^{-3}
Supersonic	0.55	0.59	0.58	1.4×10^{-2}

Figure 36: Statistics on the values of $\hat{f}$ for both loading cases.

The reason why there are slight differences between generations on the value of $\hat{f}$ is because the model is being optimized for the wrong reasons: the merged wing caused the skin and stiffeners to be the primary load bearing structures when they should not be.

Conclusion

The most significant finding from our analysis is that our simulation setup (merging all the components together) led into results that were erroneous in relation to our initial objective. This is evidenced not by our optimized design not behaving properly, but also because our "optimized" solutions lie inside the existing Pareto Frontiers. The way aerodynamic loading and structural contacts were handled resulted in an wing that had to take in considerations that initially weren't in mind (e.g. the potentially immense skin deformation , instead of overall structure deformation). This led not only to an overengineered wing (also a courtesy of bound values outside an ideal domain) but also to a wing that deformed/behaved incorrectly. The way the wing was merged made the skin and the stringers to be the primary load bearing structures, instead of the spars (evidenced in **Figure 37**). Probing the values for a supersonic case, (near the

wing's root) the spar measured a stress of 2452 psi, while a stringer read 4078 psi along the same latitude.

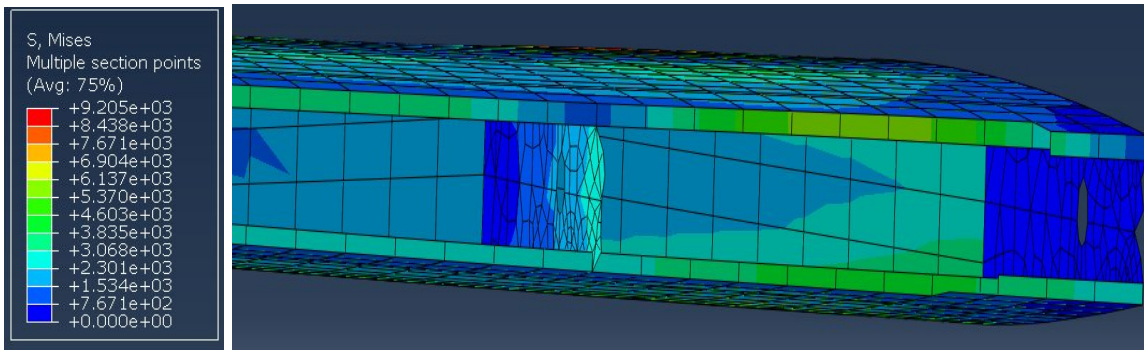

Figure 37: Wing Cross Section

Going forward, an engineering team should not merge the entire wing as we did and instead assign appropriate ties to the different parts (make the spars the master and the skin and ribs slave to the spars). In addition, a more accurate loading should be obtained from a more thorough elliptical loading expression (that maxes out at c/4 and tapers off at the trailing edge) instead of the step loads that were implemented in this analysis (another good source of loading would be to implement the wing in XFLR and get the appropriate wing loading from there). Assuming that future FEA setups prove that the stiffeners aren't part of the main load bearing structure, the respective material of those stiffeners may be changed to a lighter material (enough to guarantee no skin buckling) at the discretion of future teams. Finally, the trailing edge could be smoother than modeled in this analysis, eliminating the corner (where the max stress existed in all of our models) and allowing for the max stress to be in a more realistic location (near c/4).